ELSEVIER

Biophysical Chemistry 120 (2006) 96 – 105

Biophysical Chemistry

http://www.elsevier.com/locate/biophyschem

Rate of iron transfer through the horse spleen ferritin shell determined by the rate of formation of Prussian Blue and Fe-desferrioxamine within the ferritin cavity

Bo Zhang [a], Richard K. Watt [b], Natividad Gálvez [c], José M. Domínguez-Vera [c,*], Gerald D. Watt [a,*]

[a] *Department of Chemistry and Biochemistry, Brigham Young University, Provo, UT 84602, United States*
[b] *Depatment of Chemistry and Biochemistry, University of New Mexico, Albuquerque, NM 87131, United States*
[c] *Departamento de Química Inorgánica, Facultad de Ciencias, Universidad de Granada, 18071, Granada, Spain*

Received 24 August 2005; received in revised form 4 October 2005; accepted 5 October 2005
Available online 28 November 2005

Abstract

Iron (2+ and 3+) is believed to transfer through the three-fold channels in the ferritin shell during iron deposition and release in animal ferritins. However, the rate of iron transit in and out through these channels has not been reported. The recent synthesis of $[Fe(CN)_6]^{3-}$, Prussian Blue (PB) and desferrioxamine (DES) all trapped within the horse spleen ferritin (HoSF) interior makes these measurements feasible. We report the rate of Fe^{2+} penetrating into the ferritin interior by adding external Fe^{2+} to $[Fe(CN)_6]^{3-}$ encapsulated in the HoSF interior and measuring the rate of formation of the resulting encapsulated PB. The rate at which Fe^{2+} reacts with $[Fe(CN)_6]^{3-}$ in the HoSF interior is much slower than the formation of free PB in solution and is proceeded by a lag period. We assume this lag period and the difference in rate represent the transfer of Fe^{2+} through the HoSF protein shell. The calculated diffusion coefficient, $D \sim 5.8 \times 10^{-20}$ m^2/s corresponds to the measured lag time of 10–20 s before PB forms within the HoSF interior. The activation energy for Fe^{2+} transfer from the outside solution through the protein shell was determined to be 52.9 kJ/mol by conducting the reactions at 10~40 °C. The reaction of Fe^{3+} with encapsulated $[Fe(CN)_6]^{4-}$ also readily forms PB in the HoSF interior, but the rate is faster than the corresponding Fe^{2+} reaction. The rate for Fe^{3+} transfer through the ferritin shell was confirmed by measuring the rate of the formation of Fe-DES inside HoSF and an activation energy of 58.4 kJ/mol was determined. An attempt was made to determine the rate of iron (2+ and 3+) transit out from the ferritin interior by adding excess bipyridine or DES to PB trapped within the HoSF interior. However, the reactions are slow and occur at almost identical rates for free and HoSF-encapsulated PB, indicating that the transfer of iron from the interior through the protein shell is faster than the rate-limiting step of PB dissociation. The method described in this work presents a novel way of determining the rate of transfer of iron and possibly other small molecules through the ferritin shell.

Keywords: Iron transfer; Ferritin shell; Prussian Blue; Fe-desferrioxamine; Kinetics

1. Introduction

Ferritins are universal iron storage and detoxification proteins found in biological systems. They are usually composed of 24 subunits that pack into a spherical shell forming a hollow cavity 7–8 nm in diameter. Iron is stored in the central cavity in the form of a hydrous ferric oxide mineral core [1–6]. The internal cavity is connected to the outside solution through eight hydrophilic and six hydrophobic channels along the three-fold and four-fold axes of the protein shell. The three-fold hydrophilic channels are believed to be the pathways for iron and other molecules to enter and leave the protein interior during iron deposition and release [3,7]. Six negatively charged residues (Asp131 and Glu134) are near the center of each 3-fold channel, which are highly conserved in all animal ferritins. Biochemical, mutational and crystallographic data indicate that several metal binding sites are located in the hydrophilic three-fold channels [8,9]. The crystal structure of ferritin shows that three divalent cations can occupy this region indicating the presence of strong binding sites in the channel. Furthermore, mutation of D131 and

* Corresponding authors. José M. Domínguez-Vera is to be contacted at Tel.: +34 958 248097; fax: +34 958 248526. Gerald D. Watt, Tel.: +1 801 4224561; fax: +1 801 4220153.
E-mail addresses: josema@ugr.es (J.M. Domínguez-Vera), gdwatt@chem.byu.edu (G.D. Watt).

0301-4622/$ - see front matter © 2005 Elsevier B.V. All rights reserved.
doi:10.1016/j.bpc.2005.10.005

E134 lining the threefold channels were shown to significantly slow the rate of iron uptake [8,10] and blocking of the channel with Cr(TREN) complex also interrupted the iron entry into ferritin interior [11,12]. Model studies using the Poisson–Boltzmann equation revealed that the threefold channel is responsible for the transit of Fe^{2+} ions while the fourfold channel is basically impermeant [13,14]. These results are consistent with the threefold channels being the Fe^{2+} pathway during iron deposition and release in ferritin.

Recently Yang and Chasteen clarified the diffusional characteristics of the protein shell of horse spleen ferritin (HoSF)[1] toward small organic molecules by reporting the kinetics of permeation and effusion of nitroxide spin probes through the ferritin channels [15,16]. Their detailed analysis established that: 1) movement through the channels is a slow (20–60 min), charge-selective process, which favors positive or polar diffusants but not negative ones; 2) channel permeation and effusion are first order processes; 3) large activation energies are found for movement through the protein shell; 4) consistent with other results, diffusion into the ferritin interior occurs through the 3-fold channels and 5) specific binding to the mineral core or channel sites impeded the net transfer of nitroxide diffusants, which associated with the ferritin sites. However, while restricting large and negatively charged molecules, the negative charged behavior of the three-fold channel is expected to enhance the transfer of positively charged species such as Fe^{2+} and Fe^{3+} into and out of the mineral core. This prediction was supported by kinetic studies of Fe^{2+} release to bipyridine from the pre-reduced Fe^{2+} mineral core contained within the interior of *Azotobacter vinelandii* bacterioferritin (AvBF) [17]. Under these conditions, the rapid rate of Fe^{2+} chelation was dependent on the rate of Fe^{2+} transfer from the reduced mineral core to the chelator on the AvBF exterior. While suggestive that Fe^{2+} transfer to the outside of AvBF is rapid, this result is complicated because the rate of Fe^{2+} release occurred from a stable phosphohydroxy Fe^{2+} core present in the AvBF. These additional components could retard the rate of Fe^{2+} release so the measured rate may not correspond directly to the rate for transfer of unencumbered Fe^{2+} through the protein shell. Similar results would be expected for Fe^{2+} chelation from reduced animal ferritin cores [18,19]. The rate of Fe^{2+} and Fe^{3+} transfer through the animal and bacterioferritin shell is an important aspect of ferritin function and one in need of elucidation.

Recently the synthesis of nanoparticles of Prussian blue (PB) and Fe(III)-desferrioxamine (FeDES) in the interior of HoSF was reported [20,21], which provides a basis for measuring the rate of iron (2+ and 3+) transfer from the exterior solution through the ferritin shell to the interior cavity. To form PB within the HoSF interior, hexacyanoferrate(III) ($[Fe(CN)_6]^{3-}$) was first trapped within the ferritin by dissociating the 24-subunit apoferritin structure into its individual subunits at low pH and then reassembling the protein in the presence of high concentrations of $[Fe(CN)_6]^{3-}$ at pH 7.0. Once $[Fe(CN)_6]^{3-}$ was trapped, aliquots of Fe^{2+} solution were added to the $[Fe(CN)_6]^{3-}$ loaded HoSF (HoSF–$[Fe(CN)_6]^{3-}$) and PB formed spontaneously within the HoSF interior (HoSF–PB). Up to 100 $[Fe(CN)_6]^{3-}$ were reported to be accommodated within the HoSF interior by this process [20]. Similarly HoSF with DES and Fe(III)-DES encapsulated in the cavity (HoSF–DES, HoSF–FeDES) was synthesized by using the dissociation–reassembly method followed by addition of Fe^{3+} to the external solution of DES-loaded ferritin. Formation of PB and Fe(III)-DES in the HoSF interior was verified by UV-vis, IR spectroscopy and TEM imaging [20,21].

Following the same procedures, we report measurements of the rate of Fe^{2+} reacting with HoSF–$[Fe(CN)_6]^{3-}$, and Fe^{3+} reacting with HoSF–DES to form encapsulated PB or Fe(III)-DES. The rate of development of these complexes in the HoSF interior should be the combination of two kinetic events: 1) the rate of iron (Fe^{2+} or Fe^{3+}) entry through the protein shell into the HoSF interior and 2) the rate of iron (Fe^{2+} or Fe^{3+}) combining with $[Fe(CN)_6]^{3-}$ or DES within the aqueous confines of the HoSF interior. We assume that this second kinetic event can be determined precisely by reaction of iron with $[Fe(CN)_6]^{3-}$ or DES when both are free in solution. In a similar way, the rate of iron egress from the HoSF interior can be measured by dissociating HoSF–PB with excess 2, 2′-bipyridine (bipy) or DES. This dissociation reaction can also be viewed as consisting of two kinetic events: 1) dissociation of PB into Fe^{2+} and $[Fe(CN)_6]^{3-}$ within the HoSF interior and 2) transport of Fe^{2+} through the protein shell to the exterior solution, where it forms $[Fe(bipy)_3]^{2+}$ with excess bipyridine. In the case of Fe^{3+} egress, PB first dissociates into $[Fe(CN)_6]^{4-}$ and Fe^{3+} which transits out from the ferritin interior and reacts with DES in the exterior solution.

Using these procedures, we measured the rate of Fe^{2+} entry into the HoSF interior during formation of PB within the HoSF interior. The process of Fe^{3+} entry was also measured and occurs slightly faster than Fe^{2+}. For both reactions, a delay time was observed (10–20 s for Fe^{2+} and 5–10 s for Fe^{3+}), which corresponded to passage of the iron ions through the protein shell. The slow rate of dissociation of PB into its constituent ions prevented the determination of the rate of effusion of the iron ions from the HoSF interior.

2. Materials and methods

HoSF, Fe(III)-perchlorate hydrate, DES and bipy were purchased from Sigma-Aldrich and $K_3Fe(CN)_6$, $K_4Fe(CN)_6$ and $FeSO_4{\cdot}7H_2O$ from J. T. Baker. HoSF with $[Fe(CN)_6]^{3-}$, $[Fe(CN)_6]^{4-}$ and DES in its interior (HoSF–$[Fe(CN)_6]^{3-}$, HoSF–$[Fe(CN)_6]^{4-}$, and HoSF–DES, respectively) were prepared [20,21] and stored at 4 °C. All HoSF solutions with entrapped molecules were centrifuged prior to optical or stopped-flow measurements described below to remove small amounts of precipitate. HoSF after dissociation and re-association of subunits completely reforms the 24-mer [22,23] and was active in the iron deposition reaction. The protein concentration was determined by the Lowry method

[1] Abbreviations: HoSF, horse spleen ferritin; HoSF–$[Fe(CN)_6]^{3-}$ or HoSF–$[Fe(CN)_6]^{4-}$, HoSF with ferricyanide or ferrocyanide in the interior; HoSF–PB, HoSF with Prussian Blue in the interior; DES, desferrioxamine; bipy, 2,2′-bipyridine.

and the ferricyanide or ferrocyanide content trapped within HoSF was determined as Fe by an Inductively Coupled Plasma (ICP) spectrometer (Optima 2000). Stock solutions of bipy (0.04 M), DES (0.01 M), $FeSO_4{\cdot}7H_2O$ (6.66 mM), $Fe(ClO_4)_3$ (3.0 mM) and $K_3Fe(CN)_6$ (0.01 M) were prepared in MilliQ water, and the $K_3Fe(CN)_6$ concentration was determined optically at 420 nm ($\varepsilon = 1020\ M^{-1}\ cm^{-1}$). Reactions involving oxygen sensitive reagents were conducted in a Vacuum Atmospheres glove box with $O_2 < 1.0$ ppm (Nyad O_2 monitor). Except for the activation energy measurements all other experiments were conducted at 23 °C.

2.1. Prussian Blue (PB)

Two types of PB are recognized: soluble and insoluble [24,25]. Soluble PB is formed when limiting Fe^{2+} reacts with excess $[Fe(CN)_6]^{3-}$ and insoluble PB is formed when excess Fe^{2+} reacts with limiting $[Fe(CN)_6]^{3-}$. In all experiments reported here, soluble PB was formed. The extinction coefficient of soluble PB at 690 nm ($\varepsilon_{690nm} = 10{,}000\ M^{-1}\ cm^{-1}$) was determined by mixing a 0.01 M $FeSO_4$ solution in 1 mM HCl with a slight excess of $K_3Fe(CN)_6$. The extinction coefficient was valid up to 0.1 mM PB. Spectra of $[Fe(CN)_6]^{3-}$, $[Fe(bipy)_3]^{2+}$ and PB were measured using a HP-8453 diode array spectrophotometer and are shown in Fig. 1. Because only PB absorbs with a broad maximum at 690 nm, most of our measurements were monitored at this wavelength.

PB solutions were centrifuged at 20 °C in parallel with holo HoSF containing ~2000 Fe/HoSF at various centrifugation speeds using a Beckman Ti 70 rotor to approximate the aggregate size of PB. Additional centrifugation measurements through Nanosep filters with MW cut-off values of 30, 100 and 300 kDa were conducted to also evaluate the aggregate size of PB under the conditions of the kinetic experiments.

2.2. Kinetic measurements

2.2.1. Background

To analyze the transport of Fe^{2+} into the HoSF interior we followed a modified procedure outline by Yang and Chasteen [16]. Eq. (1) describes the process for Fe^{2+} permeation into and effusion from the HoSF interior, where $[Fe^{2+}]_o$ and $[Fe^{2+}]_i$ are the Fe^{2+} concentrations in the exterior solution and in the HoSF interior, respectively.

$$[Fe^{2+}]_o \rightleftarrows [Fe^{2+}]_i. \quad (1)$$

The rate of molecular transfer into or out of the HoSF interior was shown to be independent of the HoSF concentration [15,16]. Yang and Chasteen considered both the diffusion in and out of the ferritin interior, but a simplification results from our approach because Fe^{2+} rapidly reacts with the encapsulated $[Fe(CN)_6]^{3-}$ to form PB. This PB "sink" causes the $[Fe^{2+}]_i$ concentration to approach zero, which eliminates the back reaction due to the effusion process. The rate law for Fe^{2+} entry under these conditions is given by the forward reaction shown in Eq. (2), which is a simple first order equation for Fe^{2+} diffusion to the HoSF interior.

$$d[Fe^{2+}]_i/dt = k[Fe^{2+}]_o. \quad (2)$$

2.2.2. Kinetic procedures

Kinetic measurements for formation of free PB and PB in the HoSF interior were conducted using an Applied Photophysics stopped-flow instrument enclosed in a Vacuum Atmospheres glove box under N_2 at <1.0 ppm O_2. In each case $[Fe(CN)_6]^{3-}$ was kept constant and in >10-fold excess at pH ~7.0 with variation in the Fe^{2+} concentration. For the formation of the HoSF–PB, syringe A contained HoSF–$[Fe(CN)_6]^{3-}$ ([HoSF] = 10.2 μM, $[Fe(CN)_6]^{3-}$ = 1.03 mM, ~100$[Fe(CN)_6]^{3-}$/HoSF) and syringe B contained 5~15 μL of 6.66 mM Fe^{2+} that was diluted in 1 mL H_2O so the final Fe^{2+} concentration ranged from 0.023 to 0.050 mM. Time courses of PB formation in the HoSF interior were recorded at 690 nm over 200 s. For free PB formation $K_3Fe(CN)_6$ (0.85 mM) and different concentrations of Fe^{2+} (0.016 to 0.096 mM) were mixed and the absorbance change at 690 nm was recorded over 20 s. The kinetic curves of both free PB and HoSF–PB formation were fit with exponential functions using Microsoft Excel and the rate constants calculated. The reaction between Fe^{3+} and free or encapsulated $[Fe(CN)_6]^{4-}$ was conducted similarly with $[Fe(CN)_6]^{4-}$ at constant and excess concentration, except that Fe^{3+} reacts with free $[Fe(CN)_6]^{4-}$ too fast to be recorded on the stopped-flow instrument (dead time ~0.5 ms).[2] The rate of reaction between Fe^{3+} and HoSF–$[Fe(CN)_6]^{4-}$ ([HoSF] = 11.9 μM, $[Fe(CN)_6]^{4-}$ = 0.45 mM) is thus considered to be dependent solely on the rate of Fe^{3+} transfer through the ferritin protein shell.

The rate for Fe^{3+} penetrating the ferritin shell was verified by comparing the reaction rates of Fe^{3+} with free or DES encapsulated in HoSF. In this case, DES, either free in solution or entrapped in HoSF, was kept constant and in excess, while

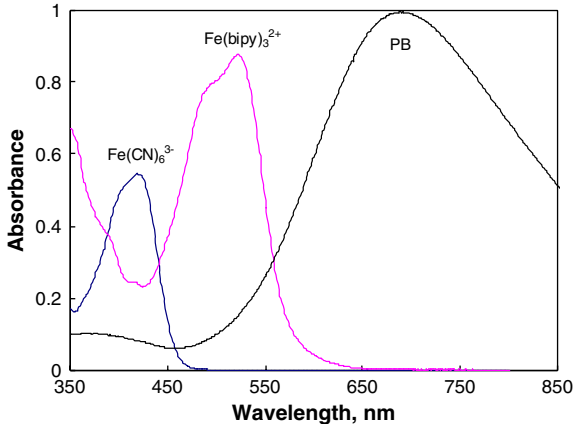

Fig. 1. Optical spectra of 0.1 mM PB, 0.1 mM $Fe(Bipy)_3^{2+}$ and 0.5 mM $K_3Fe(CN)_6$. At 690 nm, only PB absorbs strongly.

[2] Prussian Blue is also formed by the reaction of Fe^{3+} with the ferrocyanide ion ($[Fe(CN)_6]^{4-}$): $Fe^{3+} + [Fe(CN)_6]^{4-} = PB$. PB formed by both reactions is $KFe^{III}[Fe^{II}(CN)_6]$, so its formation from Fe^{2+} and $[Fe(CN)_6]^{3-}$ requires an internal electron transfer step from Fe^{2+} to $[Fe(CN)_6]^{3-}$, i.e., $Fe^{II}[Fe^{III}(CN)_6]^- = Fe^{III}[Fe^{II}(CN)_6]^-$, that does not occur when Fe^{3+} reacts with $[Fe(CN)_6]^{4-}$. This electron transfer step must limit the rate of PB formation from Fe^{2+} and $[Fe(CN)_6]^{3-}$ (24, 28).

Fe^{3+} concentration was changed to obtain a pseudo-first order rate constant with respect to Fe^{3+}. For Fe^{3+} and DES both free in solution, DES (1 mM after mixing) in one syringe was mixed with Fe^{3+} as $Fe(ClO_4)_3$ (0.03~0.09 mM after mixing) in another and the formation of the product Fe(III)-DES was monitored optically at 430 nm (ε=2865 M^{-1} cm^{-1}). In a parallel experiment, HoSF–DES ([HoSF]=5.4 μM, [DES]=0.53 mM) was mixed with Fe^{3+} (0.015~0.05 mM after mixing) and the absorbance change at 430 nm was recorded over 200 s on a stopped-flow kinetic instrument.

PB dissociation in the presence of bipy or DES was recorded on a diode array HP-8453 spectrophotometer. For free PB 2~10 μL of 0.01 M PB was diluted into 1 mL with MilliQ H_2O (pH 7.0) in an optical cell and then 30 μL of 0.04 M bipy was added and the disappearance of the blue color of PB was monitored optically at 690 nm over 150 min. The dissociation of encapsulated PB in HoSF in the presence of bipy was conducted under the same conditions except the PB in the HoSF interior (made by Fe^{2+} reacting with HoSF–$[Fe(CN)_6]^{3-}$, ~100 PB/HoSF) was 0.033 mM. The rate constants of dissociation of both free PB and HoSF–PB were obtained by fitting the kinetic curves to an exponential function.

2.3. Activation energy measurements

The activation energies of PB formation in solution and in the HoSF interior were measured on the stopped-flow instrument with temperature controlled using a NESLAB, LES-111 water-bath temperature controller. For these reactions, a 0.26 mM $[Fe(CN)_6]^{3-}$ or HoSF–$[Fe(CN)_6]^{3-}$ solution was mixed with 0.025 mM Fe^{2+} at 10~40 °C at pH 7.0. Traces of absorbance change at 690 nm were fit with exponential functions to determine the rate constant at each temperature and from their variation with temperature, the activation energy, the activation enthalpy and activation entropy were calculated from the Arrhenius plot and the Eyring equation.

$$\ln\left(\frac{kh}{k_B T}\right) = -\frac{\Delta H^{\neq}}{RT} + \frac{\Delta S^{\neq}}{R}. \quad (3)$$

The activation energies for Fe^{3+} and DES, free or inside HoSF, reaction were determined by conducting the reaction at 15, 23, 30 and 36 °C, respectively. Generally, 1.0 mM DES was mixed with 0.073 mM Fe^{3+}, while 0.11 mM HoSF–DES was mixed with 0.032 mM Fe^{3+} and the absorbance change at 430 nm recorded. The data were transported to Micro Excel and the activation energy was then calculated from the Arrhenius plot.

3. Results

3.1. Fe(II) transfer through the ferritin shell

3.1.1. Free PB formation

Fig. 2 shows the kinetic curves for PB formation free in solution at different Fe^{2+} concentration with $[Fe(CN)_6]^{3-}$ in excess. The reactions are rapid and are generally finished in <1 s. The initial rates vary linearly as a function of increasing Fe^{2+} concentration, establishing a pseudo first order Fe^{2+} dependence. When Fe^{2+} concentration was kept constant pseudo-first-order behavior in $[Fe(CN)_6]^{3-}$ was also observed. From these results, we calculated a second-order rate constant of 6.93×10^3 M^{-1} s^{-1} for reaction (4) at pH 7.0 and 23 °C.

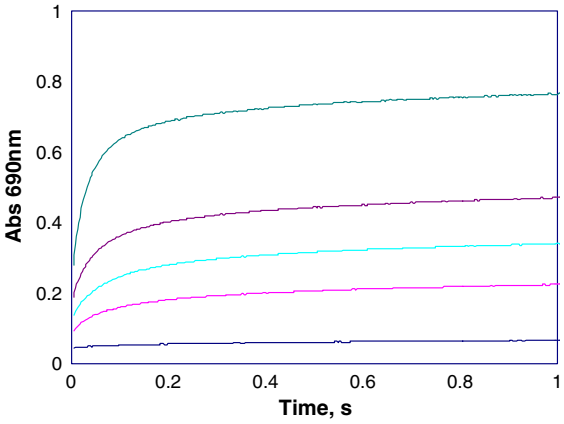

Fig. 2. Time dependence of PB formation free in solution at pH 7.0 and 23 °C measured by stopped-flow spectrophotometry. 0.85 mM $K_3Fe(CN)_6$ was mixed with 0.016, 0.032, 0.048, 0.064 and 0.096 mM Fe^{2+} (bottom to top) and the absorbance change was monitored at 690 nm.

$$K_3Fe(CN)_6 + FeSO_4 = KFe[Fe(CN)_6] + K_2SO_4. \quad (4)$$

Reaction (4) was also conducted as a function of temperature as shown in Fig. 3. At temperatures <25 °C, the kinetic curves became slightly more complex and two exponentials were required to fit the data because a slow step not observed at the higher temperatures becomes measurable but its amplitude is small, indicating only a minor reaction. The progress curves were fit by Eq. (5) from which k_1 for the fast and k_2 (only significant at 15 °C) for the slow step were obtained and the variation of k_1 as a function of temperature was plotted in the inset of Fig. 3. The activation energy, enthalpy and entropy of 24.4 kJ/mol, 21.9 kJ/mol and −86.6 J/Kmol, respectively, were calculated using Eq. (3) and compiled in Table 1.

$$A = A_0 + A_1 e^{-k_1 t} + A_2 e^{-k_2 t}. \quad (5)$$

The nature of the soluble, free PB formed in this study was further investigated by centrifugation and other methods to estimate the MW of the PB particles so that comparisons could be made with PB formed within the HoSF interior. Although soluble PB solutions at 0.010 M or higher do not precipitate after months of standing, they are aggregates (colloids) containing large numbers of iron atoms [25]. To gain some qualitative insight into the size of these aggregates, 0.01 M PB solutions and holo ferritin solutions (containing ~2000 Fe/HoSF) at ~2 mg/mL (~5 μM) were centrifuged at 20 000–45 000 rpm for 0.5 to 1.5 h in a Beckman Ti 70 rotor. In both cases, the total Fe concentration was ~0.01 M and the PB and holo HoSF sedimented nearly identically, indicating both contained molecular masses above 400 kDa. However, when completely sedimented, holo HoSF formed a clear supernatant and a dark brown pellet; whereas, PB formed a dark blue pellet but also a light blue supernatant solution above the pellet. The

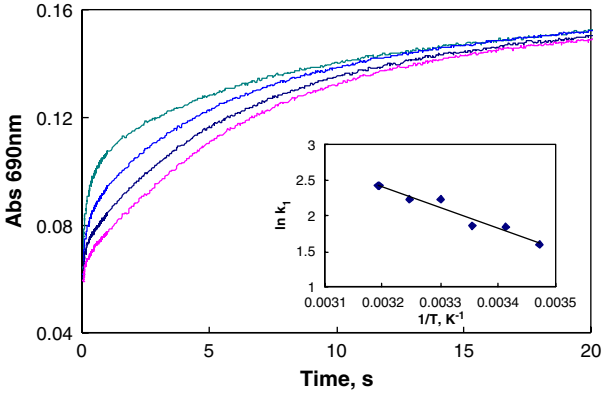

Fig. 3. Temperature variation of the rate of free PB formation at 20, 25, 30, 35 °C, bottom to top. Conditions were: 0.26 mM $[Fe(CN)_6]^{3-}$, 0.025 mM Fe^{2+}, pH 7.0. Inset: Arrhenius plot.

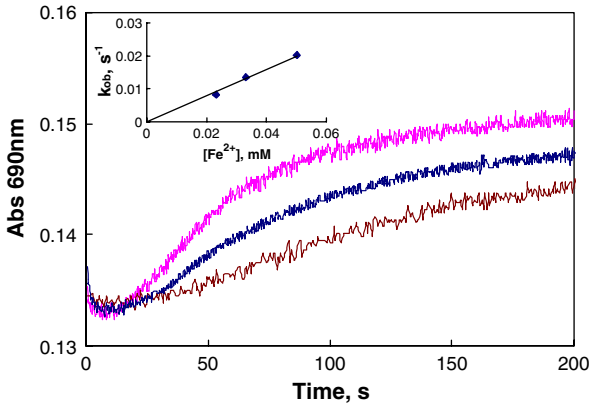

Fig. 4. Time dependence of PB formation in the HoSF interior at pH 7.0 and 23 °C measured by stopped-flow spectrophotometry. HoSF–$[Fe(CN)_6]^{3-}$ ($[Fe(CN)_6]^{3-}$=0.52 mM, [HoSF]=5.1 μM after mixing) was mixed with 0.023, 0.033, and 0.050 mM Fe^{2+} and the absorbance change monitored at 690 nm for over 200 s. Inset: first-order dependence of the observed rate constant on Fe^{2+} concentration.

presence of sedimented PB and a clear blue supernatant indicates that a heterogeneous solution of PB was initially present that leaves smaller particles in solution. Centrifugation of 0.01 M PB with centrifuge tubes containing membrane filters of 30, 100, and 300 kDa confirmed that most PB was ≥ 30 kDa because only a slight blue color came through the 30 kDa membrane filter. Dialysis with a 10 kDa membrane showed that no blue color passed through the membrane. These results suggest that although PB and holo HoSF contain similar sized aggregates, PB is more heterogeneous and significant amounts of smaller aggregates remain suspended in solution. The membrane and dialysis experiments show that even though smaller components are present they are still ≥30 kDa.

3.1.2. Formation of PB encapsulated in HoSF

As described previously [20], addition of Fe^{2+} to HoSF–$[Fe(CN)_6]^{3-}$ results in the appearance of the characteristic PB color within the HoSF interior. Based on this observation we measured the kinetics of PB formation in the HoSF interior by mixing Fe^{2+} with HoSF–$[Fe(CN)_6]^{3-}$ by measuring the change in absorbance at 690 nm as a built-in indicator of when Fe^{2+} arrives in the HoSF cavity. This is feasible because the reaction of the free ions to form PB is >1000 times faster than its formation from encapsulated $[Fe(CN)_6]^{3-}$ and Fe^{2+}, as shown in Fig. 4. Several kinetic features are evident from the formation of PB within the HoSF interior that contrast with the results in Figs. 2 and 3 for the formation of PB free in solution. First, there is a small absorbance decrease at 690 nm during the first ~5 s, which independent experiments suggested was due to Fe^{2+} reduction of oxidized centers present in HoSF because the absorbance of these oxidized centers decreases at 690 nm upon reduction [26]. The presence of oxidized centers in HoSF was previously described and are readily formed with $[Fe(CN)_6]^{3-}$ as oxidant, which is present in excess when HoSF–$[Fe(CN)_6]^{3-}$ forms [26,27]. It was not possible to pre-reduce these centers prior to Fe^{2+} addition because a low potential reductant is required, which would also reduce the encapsulated $[Fe(CN)_6]^{3-}$.

The second kinetic feature following this initial rapid absorbance decrease is that the reaction shows no absorbance increase at 690 nm during the first ~10–20 s, even though all reagents required for PB formation are present. This delay in PB formation depends on the initial Fe^{2+} concentration, with shorter delay times corresponding to higher initial Fe^{2+} concentrations (Table 2). This observed lag time is consistent with Fe^{2+} transfer across the HoSF protein shell as discussed below.

The third feature is that after this lag phase, the absorbance begins to increase with time demonstrating the formation of PB by the arriving Fe^{2+} reacting with the encapsulated $[Fe(CN)_6]^{3-}$ in the HoSF interior. First order behavior in Fe^{2+} was observed by fitting each curve to a single exponential. Good fits were obtained except for the first 10–20 s immediately after the delay time, where some deviation occurred. Further experiments show that the rate of the formation of PB in the HoSF interior is independent of the $[Fe(CN)_6]^{3-}$ concentration, suggesting the rate obeys first-order kinetics in Fe^{2+} concentration with a rate constant of 0.40 s^{-1}. This rate is much slower than that in Fig. 2 for free PB formation under similar conditions, suggesting that the rate of Fe^{2+} transfer through the HoSF shell is a first-order rate-limiting step, a result consistent with the prediction of Eq. (2).

Table 1
Activation parameters for PB and Fe^{3+}-DES formation free in solution and in the HoSF interior

Activation parameter	Free PB	HoSF–PB	Free Fe-DES	HoSF–FeDES
E_a (kJ/mol)	24.4±1.1	52.9±1.9	28.2±1.1	58.4±4.9
$\Delta H^{\neq}$ (kJ/mol)	21.9±1.2	50.5±2.0	25.7±1.2	55.9±5.1
$\Delta S^{\neq}$ (J/Kmol)	−86.6±4.6*	−120.7±4.7	−96.7±4.4*	−100.8±9.2

*$\Delta S^{\neq}$, was calculated using the second-order rate constants.

Table 2
Lag time for PB formation in HoSF interior at different iron concentrations

$[Fe^{2+}]$, mM	Lag time (s)	$[Fe^{3+}]$, mM	Lag time (s)
0.023	24	0.010	10
0.033	20	0.013	8.5
0.050	13	0.019	7.0
		0.023	6.5

To relate the observed rate constant to more fundamental quantities, we use the diffusion model derived by Yang et al. [16],

$$D = kh^2/\pi^2 \quad (6)$$

where D is the apparent diffusion constant, k is the observed rate constant and h is the thickness of the protein shell. By taking $k = 0.40\ s^{-1}$ and $h = 1.2$ nm [3], we calculated $D = 5.8 \times 10^{-20}\ m^2/s$. The delay time, t, in Fig. 4 is a measure of the time required for Fe^{2+} to traverse the protein shell, which is also related to the diffusion coefficient by the relationship $h^2 = 2Dt$. From this relationship an apparent $D = 4.8 \times 10^{-20}\ m^2/s$ is calculated using the delay time of $t = 15$ s, a result in good agreement with the D value obtained from the rate constant. The results present a consistent view of Fe^{2+} transfer being the rate-limiting step in the formation of PB within the HoSF interior. Comparing our results with those of Yang and Chasteen [16], we found that Fe^{2+} transfers ~100 times faster than nitroxide radicals, a result consistent with the difference in size and the greater positive charge on Fe^{2+} interacting with the negatively charged interior of the 3-fold channels.

The activation parameters obtained for formation of PB within the HoSF interior are $E_a = 52.9$ kJ/mol, $\Delta H^{\neq} = 50.4$ kJ/mol, $\Delta S^{\neq} = -120.7$ J/Kmol, respectively, as shown in Table 2. Since the formation of PB in the HoSF interior obeys first-order kinetics in Fe^{2+}, the activation entropy was calculated from first-order rate constants in Eq. (3). The rate constant is much larger and the activation energy much smaller for formation of PB free in solution compared to that within the HoSF interior.

3.2. Fe(III) transfer through the ferritin shell

3.2.1. Reaction of Fe(III) with free or encapsulated $Fe(CN)_6^{4-}$

The kinetics of PB formation free in solution was also measured by mixing Fe^{3+} with $[Fe(CN)_6]^{4-}$ but the rate is too fast to follow by stopped-flow spectrophotometry.[2] The equilibrium constant for reaction (7) is about 3 times larger than that for reaction (4), which partly explains the faster rate of reaction (7) [28]. Another reason is that reaction (4) likely undergoes formation of the intermediate of $KFe^{II}[Fe^{III}(CN)6]$, which then converts to the final product in reaction (7), $KFe^{III}[Fe^{II}(CN)6]$, through an internal electron transfer step [24].

$$K_4Fe^{II}(CN)_6 + Fe^{3+} = KFe^{III}[Fe^{II}(CN)_6] + 3K^+. \quad (7)$$

Time courses of PB formation within HoSF according to reaction (7) are shown in Fig. 5 and have similar kinetic characteristics as Reaction 4, shown in Fig. 4, except the lag period is shorter (Table 2). The curves after the lag period were easily fit to a single exponential confirming first order behavior in Fe^{3+}. The rate constant for reaction (7) inside HoSF is 0.76 s^{-1} ($D = 1.11 \times 10^{-19}\ m^2/s$) and is slightly larger than that for Fe^{2+} reacting with HoSF–$Fe(CN)_6^{3-}$. In addition, the kinetic traces in Fig. 5 also show an initial delay of 7~10 s ($D \sim 1.03 \times 10^{-19}\ m^2/s$) before PB begins to form, corresponding

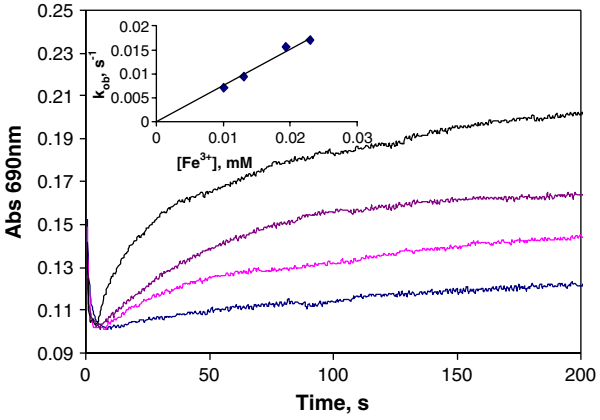

Fig. 5. Time dependence of PB formation from Fe^{3+} and HoSF–$Fe(CN)_6^{4-}$ in the HoSF interior at pH 7.0 and 23 °C. HoSF–$[Fe(CN)_6]^{4-}$ ([HoSF] = 6.0 μM, $Fe(CN)_6]^{4-}$ = 0.23 mM after mixing) was mixed with 0.010, 0.013, 0.019 and 0.023 mM Fe^{3+} (bottom to top) and the absorbance change was monitored at 690 nm over 200 s. Inset: first-order dependence of the observed rate constant on Fe^{3+} concentration.

to the faster transfer of Fe^{3+} through the HoSF shell. The reaction between free Fe^{3+} and $[Fe(CN)_6]^{4-}$ is so fast that it can be regarded as having no effect on the overall rate of PB formation, so that the measured rate is only that of Fe^{3+} transfer across the ferritin shell.

The initial decrease in absorbance at 690 nm observed in Fig. 4 is still present but cannot be explained as in Fig. 4 by the reduction of protein centers by Fe^{2+} because only Fe^{3+} is present. This rapid decrease in absorbance cannot be due to initial rapid formation of PB at another site on HoSF with subsequent decay because PB dissociation is shown later to be a very slow process.[3] The cause of this initial absorbance decrease is not known but occurs faster than the rate of transfer of Fe^{3+} into the HoSF interior and only interferes with precise measurement of the lag period.

3.2.2. Reaction of Fe(III) with DES in the absence or presence of HoSF

To verify the results of Fe^{3+} transfer through the ferritin shell obtained above, we performed another pair of parallel experiments by reacting Fe^{3+} with DES either free or encapsulated within HoSF. The reaction of Fe^{3+} with free DES is rapid with a rate constant of $1.92 \times 10^3\ M^{-1}\ s^{-1}$, while the reaction of Fe^{3+} with HoSF–DES is much slower with a rapid initial decrease in absorbance at 430 nm as in Figs. 4 and 5 and has a lag phase similar to that in Fig. 5. Following the lag phase, the reaction was shown to be first order in Fe^{3+}, with an overall rate constant of 0.74 s^{-1}, which is very close to that obtained from the Fe^{3+} and HoSF–$Fe(CN)_6^{4-}$ reaction.

The temperature variation of the reaction rates of Fe^{3+} with free DES is shown in Fig. 6 and the Arrhenius plot is shown in

[3] Another possibility for the absorbance decrease at the beginning in Figs. 4 and 5 is the initial binding of iron and O_2 to HoSF with formation and subsequent decay of the transient peroxodiiron intermediate, which has a similar rate profile at 650 nm (30–32). However because the solutions were anaerobic and the reaction conducted within a glove box with $O_2 < 0.1$ ppm, this explanation is unlikely.

the insert. The activation energy for Fe(III)-DES formation free in solution was calculated to be 28.2±1.1 kJ/mol and from separate experiments the activation energy for encapsulated HoSF–FeDES was 58.4±4.9 kJ/mol (Table 1). These values are close to the corresponding values of 24.4 and 52.9 kJ/mol for Fe^{2+} reacting with free and entrapped $[Fe(CN)_6]^{3-}$ during PB formation.

3.3. PB dissociation

3.3.1. Free PB dissociation

PB formation from Fe^{2+} and $[Fe(CN)_6]^{3-}$ and its dissociation to these ions are equilibrium processes with the formation reaction much more favorable than the dissociation reaction. However, the presence of bipy or DES can shift the equilibrium backwards by removing Fe^{2+} or Fe^{3+} through chelation.

$$Fe[Fe(CN)_6]^{-}(PB) + 3bipy = Fe(CN)_6^{3-} + Fe(bipy)_3^{2+} \quad (8)$$

$$Fe[Fe(CN)_6]^{-}(PB) + DES = Fe(CN)_6^{4-} + Fe^{3+} - DES. \quad (9)$$

The reaction of PB with excess bipy was monitored optically at 690 nm and Fig. 7 shows that PB decomposes with a rate on the order of hours even in the presence of excess iron chelator. Under these conditions, the dissociation of PB into Fe^{2+} and $[Fe(CN)_6]^{3-}$ is rate-limiting because the reaction of Fe^{2+} with bipy is very rapid [17]. Thus reaction (8) is first order in PB with a rate constant of $k_{-1}=1.27\times10^{-4}$ s^{-1} ($t_{1/2}=91$ min). For reaction (9), a first order rate constant of 1.50×10^{-4} s^{-1} was obtained under the same conditions for PB decomposition with DES (data not shown). Having measured the rate constants for both free PB formation and dissociation, the equilibrium constant for reaction (4) is calculated to be 5.46×10^{7} M. This value is comparable to a previously measured value of 1.82×10^{8} [24], indicating that the kinetic results for formation and dissociation of free PB reported here are realistic and represent the appropriate reactions.

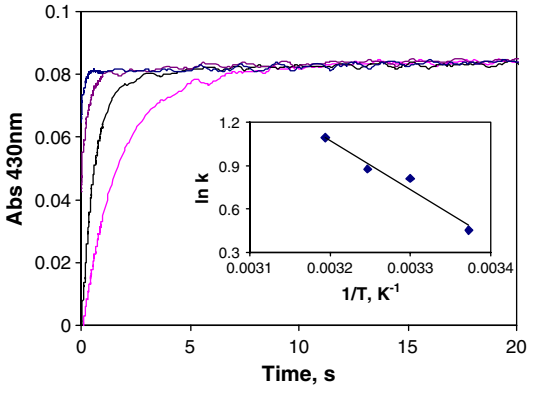

Fig. 6. Temperature variation of the rate of Fe(III)-DES formation free in solution. Conditions were: 1.0 mM DES, 0.073 mM Fe^{3+}, pH 7.0. The absorbance change was monitored at 430 nm and the reaction conducted at 15, 23, 30 and 36 °C (bottom to top). Inset: Arrhenius plot.

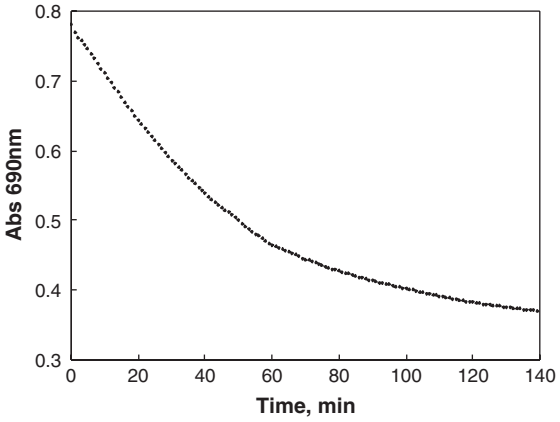

Fig. 7. Time dependence of PB dissociation in the presence of bipy at pH 7.0 and 23 °C. 30 μl of 0.04 M bipy was added to 0.97 mL of PB solution containing 0.08 mM PB and the absorbance change was monitored at 690 nm over 140 min.

3.3.2. Encapsulated PB dissociation

For HoSF–PB to be decomposed by bipy or DES, Fe^{2+} or Fe^{3+} must first dissociate from PB and then diffuse out of the ferritin interior through the threefold channels. Previous results showed that bipy or DES are too large to enter the HoSF interior [29], results consistent with recent diffusional studies of other organic molecules [15,16]. Therefore, the difference in the rate of PB dissociation in solution and that for its dissociation from HoSF–PB interior must be the transfer of iron through the channel. Addition of bipy to encapsulated PB in HoSF only caused slow formation of $[Fe(bipy)_3^{2+}]$ as evidenced by the disappearance of blue color at 690 nm, the formation of $[Fe(bipy)_3^{2+}]$ (monitored at 520 nm) and $[Fe(CN)_6]^{3-}$ (monitored at 420 nm), using the results in Fig. 1. The reaction rate is first order in HoSF–PB concentration in the presence of large excess bipy, with a rate constant of 1.17×10^{-4} s^{-1}. The kinetics of HoSF–PB dissociation with DES was similar. These results show that the rate of dissociation of PB inside the HoSF interior is rate limiting and controls the rate of external $[Fe(bipy)_3]^{2+}$ or Fe^{3+}-DES formation. Thus the passage of Fe^{2+} or Fe^{3+} from the interior to the exterior through the protein shell cannot be measured by this process.

4. Discussion

4.1. Rates of iron (2+ and 3+) transfer through the HoSF shell

Since PB formation was conducted under the same conditions free in solution or in the interior of HoSF, the differences in rate and activation parameters with and without HoSF should be due to the effect of HoSF, i.e., the transfer of iron (2+ and 3+) through the ferritin shell. The formation of free PB by Fe^{2+} and $[Fe(CN)_6]^{3-}$ or Fe^{3+} and $[Fe(CN)_6]^{4-}$ is very rapid and first-order in both reactants. The transfer of iron through the three-fold channel is a first-order rate-limiting step during the formation of PB in the HoSF interior as predicted by Eq. (2) and verified by Figs. 4 and 5. A rate constant of 0.40 s^{-1} for Fe^{2+} or 0.76 s^{-1} for Fe^{3+} was calculated for this

process. To verify this behavior with Fe^{3+}, a comparison was made for the rate of formation of PB and FeDES both inside HoSF and free in solution. The formation of free PB and FeDES are both rapid but differ significantly in rate with the reaction of Fe^{3+} and $[Fe(CN)_6]^{4-}$ being too fast to measure. However, the rates for formation of PB and FeDES from Fe^{3+} are nearly identical when the reactions are conducted within the HoSF interior under identical conditions, consistent with Fe^{3+} transfer through the HoSF shell being rate limiting.

We have assumed that the rates of PB formation inside the interior and that outside are the same but there may be small differences. A complication that could affect the rate of formation of encapsulated PB is that the highly negatively charged $[Fe(CN)_6]^{3-}$ (or $[Fe(CN)_6]^{4-}$) is confined in the small volume of the HoSF interior, which is surrounded by the inner surface of the protein shell containing negatively charged carboxylate groups. Minimizing this repulsion from the walls could cause the formation of PB to occur at a faster rate. However, any such enhancement in rate was not measurable because iron transfer through the protein shell is still the rate-limiting step. Another factor that must be considered is that because only ~100 $[Fe(CN)_6]^{3-}$ or $[Fe(CN)_6]^{4-}$ are present within the ferritin interior the size of the PB aggregates that formed is limited by this concentration constraint. In contrast the centrifugation experiments show that much larger aggregates are formed free in solution. What effect this disparity in size has upon the rates is not known.

Using spin probes (0.6–0.7 nm) slightly larger than the nominal size of the protein channels (~0.4 nm), the diffusional characteristics of permeation and effusion through the ferritin shell were elegantly described [15,16]. The major findings of those studies as outlined in the introduction were consistent with transport of the spin probes through the 3-fold channels, especially the selectivity for polar or positively charged diffusants. The observed slow transfer rates (~60 min) and high activation energies were attributed to the drag of the large organic molecules through the narrow channels. The transport of Fe^{3+} and Fe^{2+} into the HoSF interior as reported here is much faster than the large organic molecules and is consistent with their smaller size and higher positive charges, which would facilitate transfer into the interior by the known negative potential gradient arising from negative charges within the ferritin channels and the protein interior [13,14]. The negative residues near the center of the channel are believed to form intermediate binding sites, where Fe^{2+} or Fe^{3+} transiently bind during iron movement through the ferritin shell and could impede the rate of transfer into the HoSF interior. Similar behavior was noted with the positive spin probes, where a two-step process involving a nitroxide radical bound as an intermediate was required to adequately describe transfer through the channels at long incubation times [16]. If binding alone were responsible, then Fe^{3+} would be expected to transfer through the channels more slowly than Fe^{2+} but the opposite behavior is observed, suggesting other factors are involved.

Based on results presented in the introduction [8–12], we assumed that both Fe^{2+} and Fe^{3+} enter the HoSF interior via the three-fold channels but they might enter by different routes. One possibility is that Fe^{2+} enters through the ferroxidase center. During iron deposition with O_2, Fe^{2+} must transfer from the outside solution through the threefold channel to the diiron ferroxidase center where it is oxidized by O_2. The rate of formation of the diiron peroxo intermediate occurs within <50 ms, a time much shorter than that observed here (10–20 s) for overall Fe^{2+} transfer to the interior [30–32]. Although there is no O_2 present during PB formation in our experiments, it is still possible that Fe^{2+} rapidly enters the HoSF channel and then goes to the ferroxidase center where it binds tightly. If this is the case, then Fe^{2+} transfer from the ferroxidase center to the interior must be the slow step. This possibility is consistent with a very slow rate (5–10 min) of Fe^{3+} transfer from the ferroxidase center to the ferritin interior during iron deposition [33,34]. Such a pathway is complex and to further evaluate this possibility would require repeating these types of measurements with recombinant ferritins having the ferroxidase center modified to eliminate Fe^{2+} binding.

4.2. Activation parameters

The activation energy is much smaller for formation of PB free in solution compared to that within the HoSF interior. Such factors as partial or complete loss of their hydration sphere as the iron ions move into and associate with carboxyl binding sites in the channel [11,12] and energies involved in the binding and release from sites within the channel could represent a significant part of the activation energy. The activation entropies for both processes are large and negative (−86.6 vs. −120.7 J/Kmol), indicating in both cases formation of a highly ordered activated complex. However, these entropies of activation must arise from very different sources. That for formation of PB free in solution likely arises from large numbers of Fe^{2+} and $[Fe(CN)_6]^{3-}$ ions forming the PB aggregate while that for encapsulated PB likely arises from events due to passage of the Fe^{2+} through the channels. Because only ~100 $[Fe(CN)_6]^{3-}$ were present within the HoSF interior, the size of the PB particle that is formed is limited by this concentration constraint, which does not apply to the reaction free in solution.

It is interesting and perhaps significant to compare the transfer of iron ions with the transfer of the nitroxide radicals investigated earlier. A slightly higher activation energy of 63.2 ± 1.7 kJ/mol and an entropy of −66.8 kJ/mol are observed for the less charged, larger, and structurally very different nitroxide radicals. What is in common with both types of diffusants is the protein channel through which they transfer as shown in Fig. 8. The common activation parameters observed for both the larger nitroxide ions and the smaller iron ions are likely associated with the fluxional changes in the channel dimensions as previously suggested [11,19,35]. As the channels alter their dimensions the iron ions could be alternately bound and released as they move through the protein channels into the HoSF interior. The activation parameters for iron ion movement through the channels are, therefore, likely a complex combination of protein movements contributing to ion binding/release reactions.

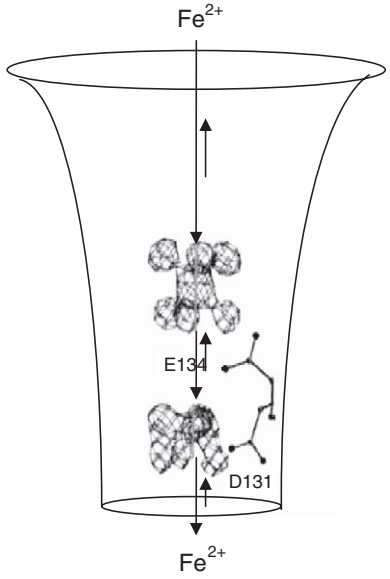

Fig. 8. Proposed mechanism for Fe^{2+} diffusion through ferritin threefold channel. The time required for Fe^{2+} pass through the channel is represented by the initial lag phase in Fig. 4. At the entrance of the funnel $[Fe(H_2O)_6]^{2+}$ ion binds to E134 and as it moves down it loses two water molecules and binds to D131 side chains. During Fe^{2+} transfer into the ferritin interior to form PB, the reverse processes shown by the short arrows are not operative due to the unidirectional nature of the reaction.

4.3. Other mechanisms and reactions

Reactions (4) and (7) showing that PB forms within the HoSF interior raises some interesting questions about the reactivity of Fe^{2+} and Fe^{3+} once they have arrived within the HoSF interior.

$$Fe^{3+} + 3OH^- \rightarrow Fe(OH)_3 \qquad K \sim 10^{38} \qquad (10)$$

$$Fe[Fe(CN)_6]^- \rightarrow Fe^{3+} + [Fe(CN)_6]^{4-} \qquad K \sim 10^{-6} \qquad (11)$$

$$Fe[Fe(CN)_6]^- + 3OH^- \rightarrow Fe(OH)_3 + [Fe(CN)_6]^{4-} \qquad K \sim 10^{32}. \qquad (12)$$

Reaction (12) shows that PB is unstable with respect to forming $Fe(OH)_3$ at pH ~8.0. Although dissociation of PB into Fe^{3+} and $[Fe(CN)_6]^{4-}$ is relatively slow (Fig. 7), it still should dissociate and form $Fe(OH)_3$ and $[Fe(CN)_6]^{4-}$ on the time scale of hours as observed when free PB is equilibrated in buffers at pH 8–11. However, PB is stable within the HoSF interior for weeks or months without $Fe(OH)_3$ formation, indicating that the HoSF interior creates conditions that prevent Reaction (12) from occurring.

Due to the size limitation of the HoSF interior, which is ~7–8 nm in diameter, and the amount of $[Fe(CN)_6]^{3-}$ actually trapped within the HoSF cavity, the size of the PB particles formed in HoSF will be limited in size and will have an aggregate size of only 200 total Fe atoms or less compared to aggregates ~7000 times larger when formed free in solution. The use of the nano-reaction cavity of HoSF is uniquely suited to prepare PB clusters of limited and presumably uniform size and could provide a means for investigating PB behavior as a function of particle size.

In summary, the present work describes a novel method of determining the kinetics of iron transfer through the ferritin shell by forming encapsulated complexes inside the ferritin. We believe that this method can be used to study the transfer of other small molecules, such as reductants, oxidants and iron chelators, through the ferritin shell by putting an appropriate indicator in the interior and then reacting it with its companion molecule that is present in the exterior solution.

Acknowledgements

NG thanks to the European Community for a Marie Curie reintegration grant (MERG-CT-2004-508033). This research was partially supported by the Department of Chemistry and Biochemistry at Brigham Young University and by grant RO202041 from the National Aeronautics and Space Administration (NASA).

References

[1] P.M. Harrison, P. Arosio, The ferritins: molecular properties, iron storage function and cellular regulation, Biochim. Biophys. Acta 1275 (1996) 161–203.
[2] P.M. Proulx-Curry, N.D. Chasteen, Molecular aspects of iron uptake and storage in ferritin, Coord. Chem. Rev. 144 (1995) 347–368.
[3] G.C. Ford, P.M. Harrison, D.W. Rice, J.M.A. Smith, A. Treffry, J.L. White, J. Yariv, Ferritin design and formation of an iron storage molecule, Philos. Trans. R. Soc. London Ser. B 304 (1984) 551–566.
[4] E.C. Theil, Ferritin structure gene regulation and cellular function in animals plants and microorganisms, Ann. Rev. Biochem. 56 (1987) 289–316.
[5] G.S. Waldo, E.C. Theil, Ferritin and Iron Biomineralization, Pergamon Press, Oxford, UK, 1996.
[6] N.D. Chasteen, P.M. Harrison, Mineralization in ferritin: an efficient means of iron storage, J. Struct. Biol. 126 (1999) 182–194.
[7] P.M. Harrison, G.C. Ford, D.W. Rice, J.M.A. Smith, A. Treffry, J.L. White, A.V. Xavier, The three-dimensional structure of apoferritin: a framework controlling ferritin's iron storage and release, Front. Bioinorg. Chem., (Lect. Int. Conf. Bioinorg. Chem.) 2nd (1986) 268–277.
[8] S. Levi, P. Santambrogio, B. Corsi, A. Cozzi, P. Arosio, Evidence that residues exposed on the three-fold channels have active roles in the mechanism of ferritin iron incorporation, Biochem. J. 317 (1996) 467–473.
[9] P.D. Hempstead, S.J. Yewdall, A.R. Fernie, D.M. Lawson, P.J. Artymiuk, D.W. Rice, G.C. Ford, P.M. Harrison, Comparison of the three-dimensional structures of recombinant human H and horse L ferritins at high resolution, J. Mol. Biol. 268 (1997) 424–448.
[10] A. Treffry, E.R. Bauminger, D. Hechel, N.W. Hodson, I. Nowik, S.J. Yewdall, P.M. Harrison, Defining the roles of the threefold channels in iron uptake, iron oxidation and iron-core formation in ferritin: a study aided by site-directed mutagenesis, Biochem. J. 296 (1993) 721–728.
[11] C.M. Barnes, E.C. Theil, K.N. Raymond, Iron uptake in ferritin is blocked by binding of $[Cr(Tren)(H_2O)(OH)]^{2+}$, a slow dissociating model for $[Fe(H_2O)(6)]^{2+}$, Proc. Natl. Acad. Sci. U. S. A. 99 (2002) 5195–5200.
[12] C.M. Barnes, S. Petoud, S.M. Cohen, K.N. Raymond, Competition studies in horse spleen ferritin probed by a kinetically inert inhibitor, $[Cr(Tren)(H_2O)(OH)]^{2+}$, and a highly luminescent Tb(III) reagent, J. Biol. Inorg. Chem. 8 (2003) 195–205.
[13] T. Takahashi, S. Kuyucak, Functional properties of threefold and fourfold channels in ferritin deduced from electrostatic calculations, Biophys. J. 84 (2003) 2256–2263.
[14] T. Douglas, R. Ripoll Daniel, Calculated electrostatic gradients in recombinant human H-chain ferritin, Protein Sci. 7 (1998) 1083–1091.

[15] X. Yang, N.D. Chasteen, Molecular diffusion into horse spleen ferritin: a nitroxide radical spin probe study, Biophys. J. 71 (1996) 1587–1595.
[16] X. Yang, P. Arosio, N.D. Chasteen, Molecular diffusion into ferritin: pathways, temperature dependence, incubation time, and concentration effects, Biophys. J. 78 (2000) 2049–2059.
[17] T.D. Richards, K.R. Pitts, G.D. Watt, A kinetic study of iron release from *Azotobacter vinelandii* bacterial ferritin, J. Inorg. Biochem. 61 (1996) 1–13.
[18] N.D. Chasteen, Ferritin. Uptake, storage, and release of iron, Met. Ions Biol. Syst. 35 (1998) 479–514.
[19] X. Liu, W. Jin, E.C. Theil, Opening protein pores with chaotropes enhances Fe reduction and chelation of Fe from the ferritin biomineral, Proc. Natl. Acad. Sci. U. S. A. 100 (2003) 3653–3658.
[20] J.M. Dominguez-Vera, E. Colacio, Nanoparticles of Prussian Blue ferritin: a new route for obtaining nanomaterials, Inorg. Chem. 42 (2003) 6983–6985.
[21] J.M. Dominguez-Vera, Iron(III) complexation of Desferrioxamine B encapsulated in apoferritin, J. Inorg. Biochem. 98 (2004) 469–472.
[22] J.L. Johnson, D.C. Norcross, P. Arosio, R.B. Frankel, G.D. Watt, Redox reactivity of animal apoferritins and apoheteropolymers assembled from recombinant and light human chain ferritins, Biochemistry 38 (1999) 4089–4096.
[23] P. Santambrogio, S. Levi, A. Cozzi, E. Rovida, A. Albertini, P. Arosio, Production and characterization of recombinant heteropolymers of human ferritin H and L chains, J. Biol. Chem. 268 (1993) 12744–12748.
[24] R.M. Izatt, G.D. Watt, H.C. Bartholomew, J.J. Christensen, A calorimetric study of Prussian Blue and Turnbull's Blue formation, Inorg. Chem. 9 (1970) 2019–2021.
[25] H.J. Buser, D. Schwarzenbach, W. Petter, A. Ludi, The crystal structure of Prussian Blue: $Fe_4[Fe(CN)_6]^{3-}\times H_2O$, Inorg. Chem. 16 (1977) 2704–2710.
[26] R.K. Watt, R.B. Frankel, G.D. Watt, Redox reactions of apo mammalian ferritin, Biochemistry 31 (1992) 9673–9679.
[27] G.D. Watt, D. Jacobs, R.B. Frankel, Redox reactivity of bacterial and mammalian ferritin: is reductant entry into the ferritin interior a necessary step for iron release, Proc. Natl. Acad. Sci. U. S. A. 85 (1988) 7457–7461.
[28] G.D. Watt, J.J. Christensen, R.M. Izatt, Thermodynamics of metal cyanide coordination. III. *G*, *H*, and *S* values for ferrocyanide and ferricyanide ion formation in aqueous solution at 25 °C, Inorg. Chem. 4 (1965) 220–222.
[29] B. Webb, J. Frame, Z. Zhao, M.L. Lee, T.D. Watt, Molecular Entrapment of Small Molecules within the Interior of Horse Spleen Ferritin, Arch. Biochem. Biophys. 309 (1994) 178–183.
[30] F. Bou-Abdallah, G. Biasiotto, P. Arosio, N.D. Chasteen, The putative "nucleation site" in human H-chain ferritin is not required for mineralization of the iron core, Biochemistry 43 (2004) 4332–4337.
[31] A. Treffry, Z. Zhao, M.A. Quail, J.R. Guest, P.M. Harrison, Iron (II) oxidation by H chain ferritin: evidence from site-directed mutagenesis that a transient blue species is formed at the dinuclear iron center, Biochemistry 34 (1995) 15204–15213.
[32] F. Bou-Abdallah, G. Zhao, H.R. Mayne, P. Arosio, N.D. Chasteen, Origin of the unusual kinetics of iorn deposition in human H-chain ferritin, J. Am. Chem. Soc. 127 (2005) 3885–3893.
[33] X. Yang, Y. Chen-Barrett, P. Arosio, N.D. Chasteen, Reaction paths of iron oxidation and hydrolysis in horse spleen and recombinant human ferritins, Biochemistry 37 (1998) 9743–9750.
[34] G. Zhao, F. Bou-Abdallah, P. Arosio, S. Levi, C. Janus-Chandler, N.D. Chasteen, Multiple pathways for mineral core formation in mammalian apoferritin. The role of Hydrogen Peroxide, Biochemistry 42 (2003) 3142–3150.
[35] H. Takagi, D. Shi, Y. Ha, N.M. Allewell, E.C. Theil, Localized unfolding at the junction of three ferritin subunits. A mechanism for iron release? J. Biol. Chem. 273 (1998) 18685–18688.